Azimuthal AVO and curvature

Jesse M. Kolb, David Cho†, and Kris Innanen

ABSTRACT

Azimuthal AVO can be used to determine anisotropic elastic parameters in the subsurface. AVO methods often separate the effects of elastic parameters on the reflection coefficient into three terms: intercept, gradient, and curvature. In this paper we show that the gradient is characterized by multiple independent terms that change with azimuth, leading to nonuniqueness when used to characterize anisotropy, while the curvature term is only influenced by a single term proportional to the change in horizontal P-wave velocity across the interface along an azimuth. This gives the curvature the capability of determining anisotropy without ambiguity and makes it a useful quantity to estimate, especially when it is combined with the gradient. Additionally, we analyze the nonlinearity present in the precritical region of large-contrast reflections and demonstrate the advantage of using exact reflection coefficients for nonlinear inversion by employing a Markov chain Monte Carlo algorithm.

INTRODUCTION

Estimation of the azimuthal variation of elastic parameters is useful for a number of reasons. For example, it can be used to improve imaging (see Tsvankin et al., 2001) and can provide information about natural fracture density and orientation (Hudson, 1981; Schoenberg and Sayers, 1995), preferred stress orientation (Prioul et al., 2004), and brittleness (Parney et al., 2010).

Methods for azimuthal AVO used in industry traditionally assume a single set of vertical fractures and HTI symmetry (e.g. Rüger, 1998), whereas most reservoirs typically contain multiple fracture sets (e.g. Gillespie et al., 1993). It has been suggested that one of the reasons these methods often fail is due to this assumption (Sayers, 2009), and accurate estimation of more general anisotropic parameters could lead to better results.

Another problem in azimuthal AVO inversions is an ambiguity in the fracture direction. The equation often used to determine the symmetry axis of an HTI medium from Rüger (1998) is nonlinear and produces two possible solutions, with two mutually perpendicular fracture orientations possible. The inversion can be reduced to a single solution if the sign of the AVO gradient is known, but as shown by Goodway et al. (2010) the sign can be negative or positive and is difficult to constrain.

In this paper we use a formulation for general anisotropy provided by Vavryčuk and Pšenčík (1998) to write the effect of stiffness coefficients along a single azimuth on the reflection coefficient along that same azimuth. Using this formulation, we show that the simplicity of the curvature allows for unique inversions, while the complexity of the gradient (it has two terms that vary with azimuth) is what causes the nonuniqueness of its

† Qeye Labs Canada

solutions.

BACKGROUND THEORY

Shuey (1985) showed that the linearized reflection coefficient for PP reflections at small incidence angles in isotropic media could be written in the form

$$R_{PP}^{iso}(\theta) = A + B\sin^2\theta + C\tan^2\theta\sin^2\theta, \tag{1}$$

where A is the normal-incidence or intercept term, B affects the slope of the reflection coefficient at small angles and is often called the gradient term, and C only affects the reflection coefficient at large angles and is called the curvature term. Thomsen (1990) used this form to describe the effect of common seismic parameters V_P, V_S, ρ, and μ on the reflection coefficient:

$$R_{PP}^{iso}(\theta) = \frac{1}{2}\left[\frac{\Delta V_P}{\overline{V}_P} + \frac{\Delta\rho}{\overline{\rho}}\right] + \frac{1}{2}\left[\frac{\Delta V_P}{\overline{V}_P} - \left(\frac{2\overline{V}_S}{\overline{V}_P}\right)^2\frac{\Delta\mu}{\overline{\mu}}\right]\sin^2\theta + \frac{1}{2}\frac{\Delta V_P}{\overline{V}_P}\tan^2\theta\sin^2\theta. \tag{2}$$

Thomsen (1993) derived the linearized PP reflection coefficient for small-contrast weak anisotropy:

$$\begin{aligned} R_{PP}(\theta) =& \frac{1}{2}\left[\frac{\Delta Z_0}{\overline{Z}_0}\right] \\ &+ \frac{1}{2}\left[\frac{\Delta V_{P_0}}{\overline{V}_{P_0}} - \left(\frac{2\overline{V}_{S_0}}{\overline{V}_{P_0}}\right)^2\frac{\Delta\mu_0}{\overline{\mu}_0} + (\delta_2 - \delta_1)\right]\sin^2\theta \\ &+ \frac{1}{2}\left[\frac{\Delta V_{P_0}}{\overline{V}_{P_0}} - (\delta_2 - \delta_1 - \epsilon_2 + \epsilon_1)\right]\tan^2\theta\sin^2\theta, \end{aligned} \tag{3}$$

where V_{P_0} and V_{S_0} are vertical P and S velocities, $Z_0 = \rho V_{P_0}$ and $\mu_0 = \rho V_{S_0}^2$ are the vertical P-wave impedance and shear modulus, and δ and ϵ are anisotropy parameters from Thomsen (1986). Δ denotes the difference in a parameter's values across the interface and the overbar denotes the average of a parameter's values on both sides of the interface. Rüger (1995) showed that equation 3 is more accurate without the δ_2 and δ_1 in the curvature.

Vavryčuk and Pšenčík (1998) calculated linearized reflection coefficients for an interface between weak, generally anisotropic media using perturbations from background P-wave velocities, α, and S-wave velocities, β, and expressed the PP reflection in a form similar to Thomsen (1993) as given below:

$$\begin{aligned} R_{PP}(\theta_P) =& \frac{\rho\Delta A'_{33} + 2\alpha^2\Delta\rho}{4\rho\alpha^2} \\ &+ \frac{1}{2}\left[\frac{\Delta A'_{33}}{2\alpha^2} - \frac{4(\rho\Delta A'_{55} + \beta^2\Delta\rho)}{\rho\alpha^2} + \Delta\delta^{*\prime}\right]\sin^2\theta_P \\ &+ \frac{1}{2}\left(\frac{\Delta A'_{33}}{2\alpha^2} + \Delta\epsilon^{*\prime}\right)\sin^2\theta_P\tan^2\theta_P \end{aligned} \tag{4}$$

where

$$\delta^{*\prime} = \frac{A'_{13} + 2A'_{55} - A'_{33}}{\alpha^2}, \epsilon^{*\prime} = \frac{A'_{11} - A'_{33}}{2\alpha^2} \tag{5}$$

and $A_{\alpha\beta}$ is Voigt notation for the density-normalized elastic parameters. The ' symbol denotes that the parameters are in the coordinate system which is rotated to be aligned with the vertical plane containing the source and receiver. Vavryčuk and Pšenčík (1998) then showed that by using a coordinate transformation, equation 4 could describe the PP reflection along any arbitrary vertical plane of incidence and reflection.

A REXPRESSION OF THE CURVATURE TERM

By substituting $\Delta\epsilon^{*\prime}$ into equation 4 and combining terms the curvature becomes

$$\frac{1}{2}\left(\frac{\Delta A'_{33}}{2\alpha^2} + \frac{\Delta A'_{11} - \Delta A'_{33}}{2\alpha^2}\right) = \frac{\Delta A'_{11}}{4\alpha^2} \approx \frac{1}{2}\frac{\Delta V'_{PH}}{\overline{V}'_{PH}}, \tag{6}$$

where V_{PH} is the horizontal P-velocity. Eq. 6 seems to be simpler to understand than the original form, at least for generally anisotropic media with no assumed symmetry axes in which the meaning of $\Delta\epsilon^{*\prime}$ is less useful. Zillmer et al. (1998) expressed the curvature in a form similar to eq. 6 but did not explicitly describe how this simplification could be used in azimuthal AVO measurements. The curvature is proportional to $\Delta A'_{11}$, the change in the square of the horizontal P-velocity along the vertical plane containing the source and receiver. This also makes it clear that curvature is not being caused by a change in vertical P-wave velocity as might be assumed by the presence of ΔV_{P_0} in the curvature of equation 3 and $\Delta A'_{33}$ in the curvature of equation 4, if one does not inspect the equations further. Also, when looking back at the isotropic reflection coefficients in equation 2 it is now clear that the ΔV_P in the intercept is the change in vertical P-wave velocity and the ΔV_P in the curvature is the horizontal P-wave velocity but since the media are isotropic they simply become the same. It should be noted that if there is anisotropy in a layer and one tries to use the curvature to separate the P-velocity and density terms from each other in the intercept term, that this could cause problems since the intercept's velocity and the curvature's velocity will not necessarily be the same.

Equation 6 is the curvature along a single plane, but a 21 parameter stiffness tensor describes all parameters in all directions and can be used to make the curvature more general

if so desired. From Bond (1943), the coordinate transformation for A'_{11} along an arbitrary vertical plane at an angle ϕ from the original plane is

$$A'_{11} = A_{11}\cos^4\phi + 4A_{16}\cos^3\phi\sin\phi + 2(A_{12}+2A_{66})\cos^2\phi\sin^2\phi + 4A_{26}\sin^3\phi\cos\phi + A_{22}\sin^4\phi. \tag{7}$$

This allows the curvature to be written as

$$\frac{1}{4\alpha^2}\left[\Delta A_{11}\cos^4\phi + 4\Delta A_{16}\cos^3\phi\sin\phi + 2(\Delta A_{12}+2\Delta A_{66})\cos^2\phi\sin^2\phi + 4\Delta A_{26}\sin^3\phi\cos\phi + \Delta A_{22}\sin^4\phi\right]. \tag{8}$$

Rüger (1998) writes the weak contrast curvature for two HTI media with the same symmetry axis as

$$\frac{1}{2}\left[\frac{\Delta\alpha}{\overline{\alpha}} + \Delta\epsilon^{(V)}\cos^4\phi + \Delta\delta^{(V)}\sin^2\phi\cos^2\phi\right] \tag{9}$$

and if we substitute the weak anisotropic parameters from Vavryčuk and Pšenčík (1998) shown in equation 5 into expression 9 and assume $\alpha^2 = A_{33}$, expression 9 becomes

$$\frac{1}{2}\left[\left(\frac{\Delta A_{33}}{2\alpha^2}\right) + \left(\frac{\Delta A_{11}-\Delta A_{33}}{2\alpha^2}\right)\cos^4\phi + \left(\frac{\Delta A_{13}+2\Delta A_{55}-\Delta A_{33}}{\alpha^2}\right)\sin^2\phi\cos^2\phi\right] = \frac{1}{4\alpha^2}\left[\Delta A_{11}\cos^4\phi + 2(\Delta A_{13}+2\Delta A_{55})\cos^2\phi\sin^2\phi + \Delta A_{33}\sin^4\phi\right]. \tag{10}$$

In media with transverse isotropy with a horizontal axis of symmetry the following are true:

$$A_{12} = A_{13}, A_{66} = A_{55}, A_{22} = A_{33}, A_{16} = A_{26} = 0, \tag{11}$$

and expression 8 can be written in the form of equation 10. Expression 8, however holds for general (weak) anisotropy and expressing the terms as A_{12}, A_{66}, and A_{22} is a good reminder that it is the horizontal stiffnesses (or velocities, depending on parameterization) affecting the curvature rather than the vertical stiffnesses even if the media has symmetry which allows the terms to be interchanged.

EXPLANATION OF AMBIGUITIES IN FRACTURE DIRECTION

Substituting $\Delta\delta^*$ into equation 4, the gradient term along a single plane is

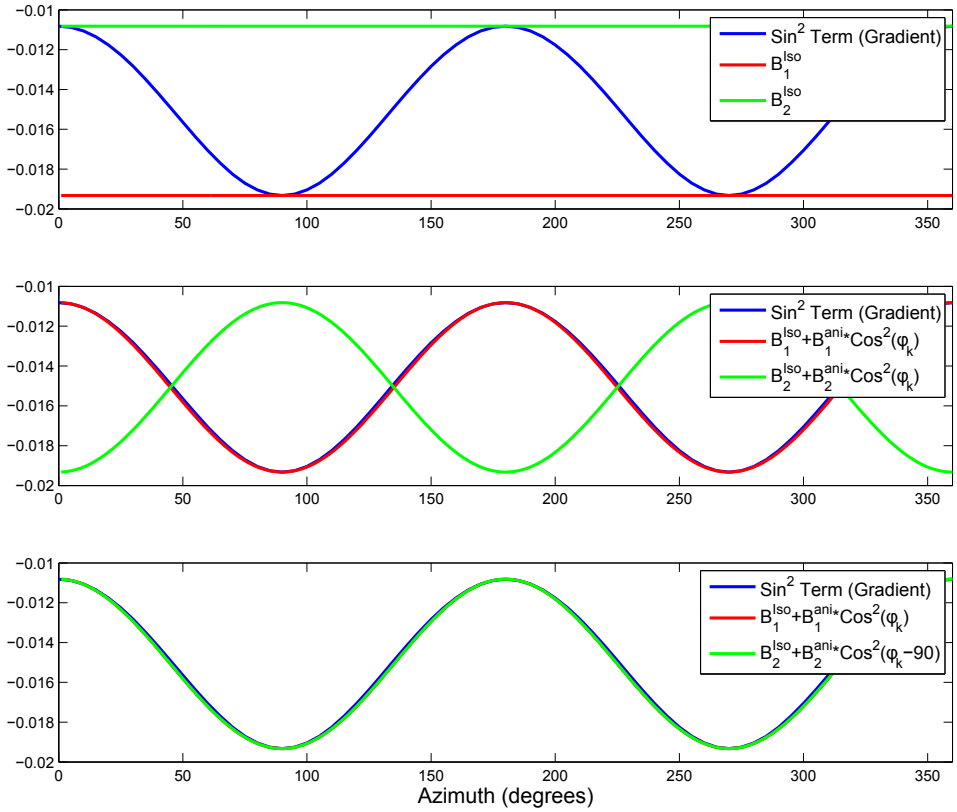

FIG. 1. Two solutions for the azimuthal AVO gradient. The azimuthal gradient for an isotropic halfspace overlaying a halfspace with HTI symmetry is shown in blue. Two different solutions for B^{iso}, B^{ani}, and ϕ_{sym} from equation 14 are shown in green and red (the values of ϕ_{sym} for the solutions are 0° and 90°). (top) Two gradient for two isotropic backgrounds along with the true gradient (middle) anisotropic perturbations are added to the isotropic backgrounds, both oriented at 0 degrees (bottom) for one of the solutions (red), the anisotropic perturbation of the gradient has to be rotated by 90 degrees (a shift of 90 degrees on this plot) to fit the true gradient. This nonuniqueness is caused in part by what is considered the isotropic response and what is considered the anisotropic deviation from that response.

$$\frac{1}{2}\left[\frac{\Delta A'_{33}}{2\alpha^2} - \frac{4(\rho\Delta A'_{55} + \beta^2\Delta\rho)}{\rho\alpha^2} + \frac{\Delta A'_{13} + 2\Delta A'_{55} - \Delta A'_{33}}{\alpha^2}\right] = \frac{1}{2\alpha^2}\left[-2\Delta A'_{55} - 4\beta^2\frac{\Delta\rho}{\rho} + \Delta A'_{13} - \frac{\Delta A'_{33}}{2}\right] \tag{12}$$

The only terms in equation 12 that change with azimuth are $\Delta A'_{55}$ and $\Delta A'_{13}$ under the following relations (from Bond (1943)):

$$\begin{aligned} A'_{55} &= A_{55}\cos^2\phi + 2A_{45}\cos\phi\sin\phi + A_{44}\sin^2\phi, \\ A'_{13} &= A_{13}\cos^2\phi + 2A_{36}\cos\phi\sin\phi + A_{23}\sin^2\phi. \end{aligned} \tag{13}$$

In Figure 1 the gradient for a model from Vavryčuk and Pšenčík (1998) (Case A and C) of an isotropic halfspace overlaying a halfspace with HTI symmetry assumed to be caused by vertical parallel dry (gas-filled) cracks taken from is shown in blue. This was calculated using the Center for Wave Phenomena's reflection coefficient code and solving a system of linear equations for the $\sin^2\theta$ term. A now commonly used parameterization of the gradient for HTI media is the gradient from "Rüger's equation" given in Rüger (1998) as

$$B(\phi_k) = B^{iso} + B^{ani}\cos^2(\phi_k - \phi_{sym}), \tag{14}$$

which allows the gradient to be broken into the contribution of the isotropic component B^{iso}, an anisotropic component B^{ani} and the symmetry axis ϕ_{sym}. Unfortunately, as shown in Figure 1 the solution to equation 14 is nonunique and there are two possible solutions, shown in red and green for the example in Figure 1. This formula is often used to attempt to determine a symmetry axis, and the two solutions have a 90 degree difference in ϕ_{sym}, so it is often said that Rüger's equation has a 90 degree ambiguity in it. Since $B_2^{ani} = -B_1^{ani}$ for the two possible solutions, if the sign of B^{ani} is known then it can be used to constrain the symmetry axis.

Another way of looking at the gradient curve's azimuthal change is simply as the fluctuations of the quantity $\frac{1}{2\alpha^2}[-2\Delta A'_{55} + \Delta A'_{13}]$ with azimuth. At least when using synthetic data, there is no ambiguity in the system; there are just minimums and maximums in the gradient corresponding to minimums and maximums in $[-2\Delta A'_{55} + \Delta A'_{13}]$. The ambiguity comes when one decides to assume that a minimum or maximum in the gradient corresponds with a symmetry axis. The problem with saying if a minimum or maximum in this term corresponds to the symmetry axis is that dry fractures will decrease both A'_{55} and A'_{13} along the symmetry axis. In fact, it can easily be seen that these terms could cancel and there could be no change in gradient with azimuth for an interface between anisotropic media.

Figure 2 from Bakulin et al. (2000) shows the change in the difference of the gradient parallel and perpendicular to fractures with Vs/Vp ratio for an isotropic halfspace over an HTI halfspace caused by fractures. They show that with their model, reasonable Vs/Vp ratios, and a crack density of .07 for dry (gas-filled) cracks it is possible to have no azimuthal change in the gradient while for wet (liquid-filled) cracks there is always a change. This makes sense because wet cracks will have minimal excess normal compliance and will not influence A_{13} or A_{23} while they will still influence the S-wave polarized along the symmetry axis changing A_{55}. For the dry cracks, which add excess normal and tangential compliance, A_{13} will be reduced and it is possible for $-2\Delta A_{55}$ and ΔA_{13} to cancel. For dry cracks, larger P-velocities, shown on the left side of Figure 2, will be more influenced by excess normal compliances, ΔA_{13} dominates the change in gradient, and the gradient along the symmetry axis will be negative, while for larger S-velocities, shown on the right side of Figure 2, excess tangential compliances will have a larger effect, $-2\Delta A_{55}$ will dominate, and the gradient along the symmetry axis will be positive. Even without knowledge of the symmetry axis (if there is one), the change of the combination of $[-2\Delta A'_{55} + \Delta A'_{13}]$ with azimuth could be a useful quantity to estimate. Also, although this example is for HTI, this change in gradient with the change in $[-2\Delta A'_{55} + \Delta A'_{13}]$ with azimuth should apply

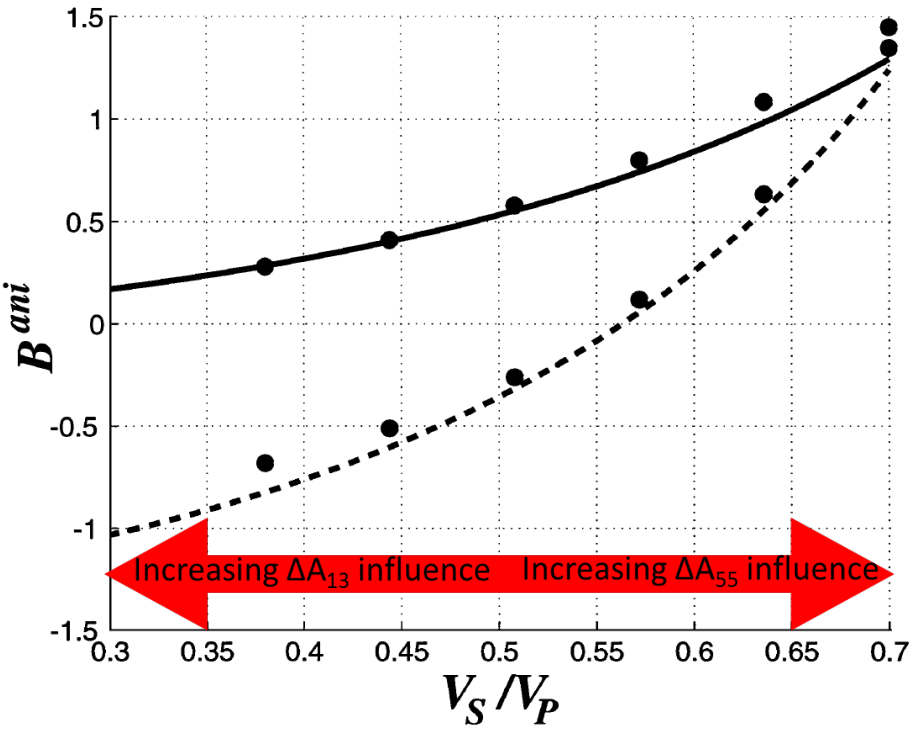

FIG. 2. Change in the anisotropic gradient with Vs/Vp ratio of the background rock in a rock with HTI symmetry due to aligned vertical fractures. The difference between the anisotropic gradient perpendicular and parallel to the cracks (B^{ani}) for wet fractures are given by the solid line and for dry fractures by the dashed line. Dots signify values of B^{ani} from the exact reflection coefficients. The red arrow shows the increasing influence of ΔA_{13} as Vs/Vp decreases, and the increasing influence of ΔA_{55} as Vs/Vp increases (figure adapted from Bakulin et al. (2000)).

to more general cases.

RESOLVING FRACTURE DIRECTION AMBIGUITY

Figure 3 shows every other azimuth of processed azimuthal AVO data from an interface between plexiglas and phenolic material, collected and processed by Faranak Mahmoudian for her thesis (Mahmoudian, 2013). Prior to azimuthal AVO tests, the stiffnesses and velocities of the materials used were estimated by Mahmoudian (2013) and are shown in Table 1 and Table 2. The plexigas is approximately isotropic and the phenolic layer is orthorhombic, but can be approximated as a medium with HTI symmetry, simulating a set of aligned fractures with the symmetry axis along the x_1-axis corresponding to an azimuth of 0°. Because in this problem the overburden is isotropic, solving for the change in parameters across the interface provides us with the anisotropy of the bottom layer.

Mahmoudian (2013) used a method outlined in Jenner (2002) that uses Rüger's equation to estimate the fracture direction. She was able to successfully estimate the correct direction with an error of just 0.8°. Unfortunately, due to the ambiguity previously mentioned, the method predicts both the correct symmetry axis, and a symmetry axis perpendicular to the true symmetry axis, and it is unclear which is correct.

We solved a system of linear equation to find the coefficients to 1, $\sin^2\theta$, and $\sin^2\theta\tan^2\theta$

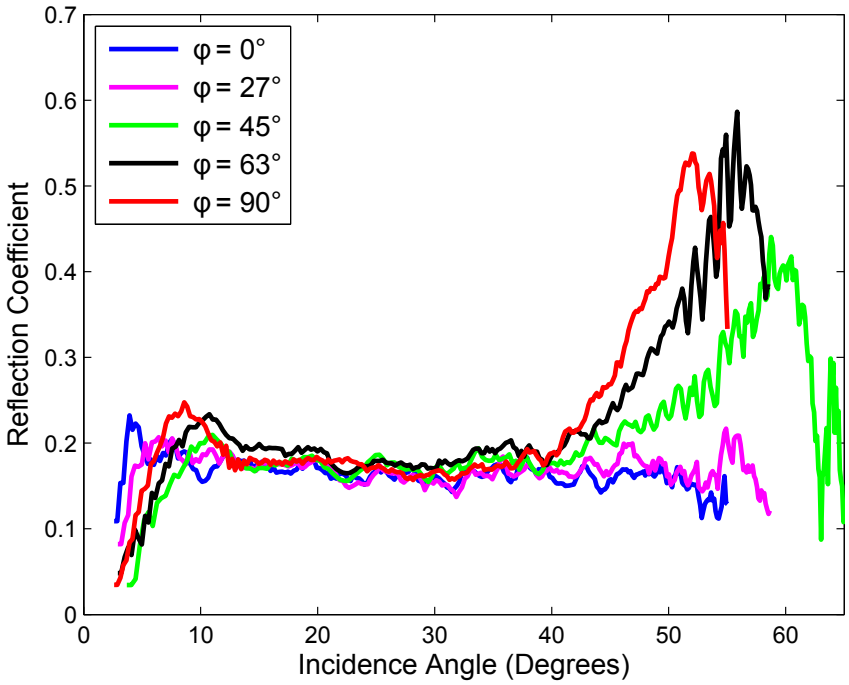

FIG. 3. Azimuthal reflection data from Mahmoudian (2013) for a physical model with elastic parameters given in Table 1 and Table 2. A small anomaly at incidence angles of $\sim$ 0-12 degrees was unable to be removed during processing. At large angles and for azimuths with faster velocities a large reflection is recorded near the critical angle.

$$\begin{bmatrix} 8.70 \pm 0.49 & 4.68 \pm 0.21 & 5.07 \pm 0.21 & 0 & 0 & 0 \\ & 13.25 \pm 0.49 & 5.13 \pm 0.23 & 0 & 0 & 0 \\ & & 12.25 \pm 0.49 & 0 & 0 & 0 \\ & & & 2.89 \pm 0.12 & 0 & 0 \\ & & & & 2.34 \pm 0.12 & 0 \\ & & & & & 2.28 \pm 0.12 \end{bmatrix}$$

Table 1. Approximate P-velocities, S-velocities, and densities for the materials used in the physical model, estimated from group velocities by Mahmoudian (2013).

	P-velocity (m/s)	S-velocity (m/s)	Density (g/cc)
Water	1485	~ 0.0	1.00
Plexiglas	2745	1380	1.19
Phenolic	3570 ($\parallel$) 2900 ($\perp$)	1700 ($\parallel$) 1520 ($\perp$)	1.39

Table 2. Approximate P-velocities, S-velocities, and densities for the materials used in the physical model, estimated from group velocities by Mahmoudian (2013).

(which are the the AVO intercept, gradient, and curvature) that best fit the data for each azimuth, and the results are shown in Figure 4. In order to do this we could only use certain incident angles because there was error at small angles which could not be removed through processing and at large angles the incidence angle is close to critical and linear equations are no longer good approximations. We chose to use angles between 12.5 and 45 degrees for these calculations. From the AVO gradient, one can tell that the likely symmetry axis is either about 0 degrees or 90 degrees due to the minimum and maximum being at those azimuths. However the gradient is made up of two terms and it is not clear whether 0 or 90 degrees is the symmetry axis. The curvature also has a minimum and maximum at 0 and 90 degrees. The difference, however, is that the gradient only consists of one term per azimuth and so we know which direction has a larger change in the horizontal velocity and which has the smaller. In this case, since the overburden is isotropic, it also tells us the fast and slow direction for the underlying layer.

Figure 5 shows a best fit of equation 8 to the measured curvature. A_{16} and A_{26} were set to zero, which assumes orthorhombic symmetry. Also, the data was only for azimuths of 0 to 90 degrees and the rest of the azimuths were filled in to make the figure easier to understand. Shifting the data by any amount and finding the angle that gives the largest difference between ΔA_{11} and ΔA_{22} shows that this is the case at 0 and 90 degrees exactly. Since there is only one term affecting the curvature, however, it is able to find that the symmetry axis is 0 degrees. This won't always be the case of course; data will often be noisier than the dataset we used, the overburden may not be isotropic, one can't necessarily assume the underlying layer is orthorhombic, and one can change the range of incidence angles to include. Regardless, the curvature seems like a reasonable way to constrain anisotropic measurements geophysicists make using the gradient, especially when there is a 90 degree ambiguity in the fracture direction.

NONLINEARITY IN THE REFLECTION COEFFICIENT

It is well known that the precritical region of reflection coefficients is increasingly more nonlinear with larger incidence angles (see Castagna and Backus, 1993). Since the AVO curvature is more sensitive to larger incidence angles than the other AVO terms, it is most affected by this nonlinearity. In Figure 4 we showed that the curvature was larger at 90 degrees azimuth, but the estimated magnitude is off by a factor of almost 3 (0.4176 estimated vs 0.1465 substituting the stiffnesses into $\frac{\Delta A'_{11}}{4\alpha^2}$). The difference between using the linearization from Vavryčuk and Pšenčík (1998) (eq. 4 in this paper) for the model we're using from Mahmoudian (2013) and the exact plane-wave equation is shown in Figure 6. The exact plane-wave equation is shown in blue, eq. 4 using all 3 angle terms in green, and eq. 4 using just the AVO intercept and AVO curvature terms in red. The solid lines are for an azimuth of 90° which is the fast direction of the lower medium, representing the direction parallel to a fractured medium. The dotted lines are for an azimuth of 0° which is the slow direction of the lower medium, representing the direction perpendicular to a fractured medium. Using the all 3 terms, including the AVO curvature, more closely approximates the exact plane-wave reflection coefficient than just using 2 terms and in the fast direction in which there is a larger contrast in velocities, the 3 term linearization diverges around 30 degrees rather than at 20 degrees. For the fast direction, in which the contrast of elastic parameters across the layer is greater, the linearizations do not approximate the exact

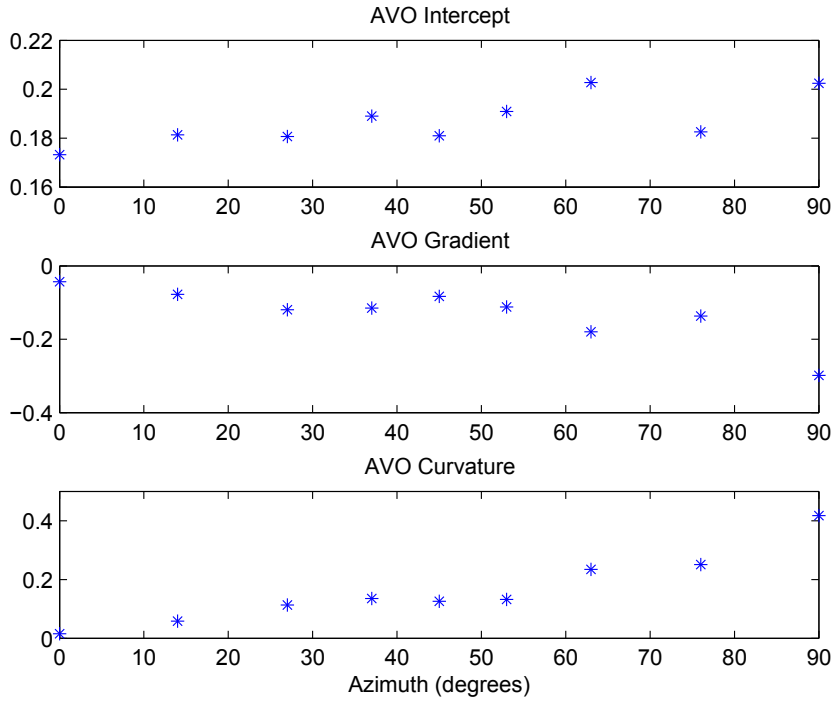

FIG. 4. Azimuthal variations in the AVO intercept, gradient and curvature. These were calculated from azimuthal reflection data shown in Figure 3.

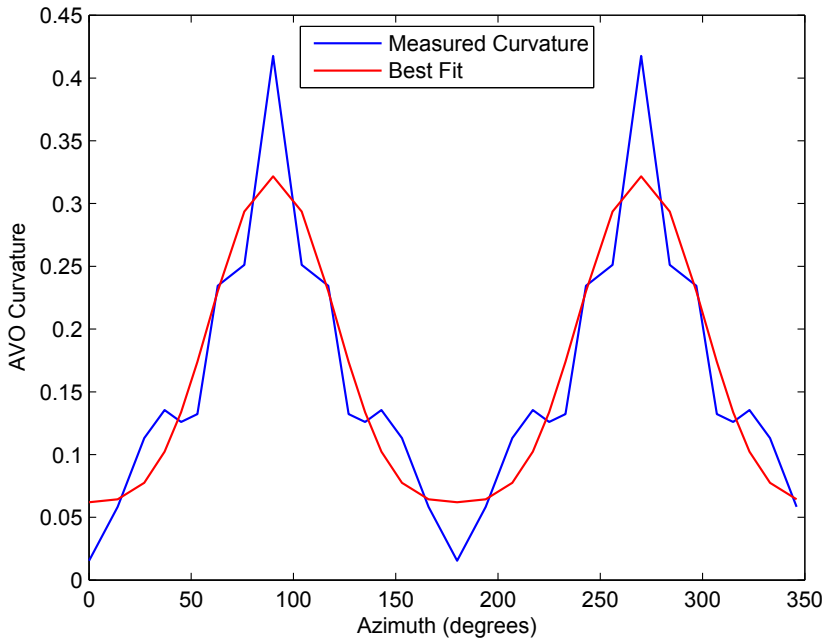

FIG. 5. Best fit of equation 8 to the curvature obtained from the data. For this particular dataset, the curvature determines the fracture symmetry axis direction exactly. For lower quality data, this analysis should still provide a constraint on anisotropy.

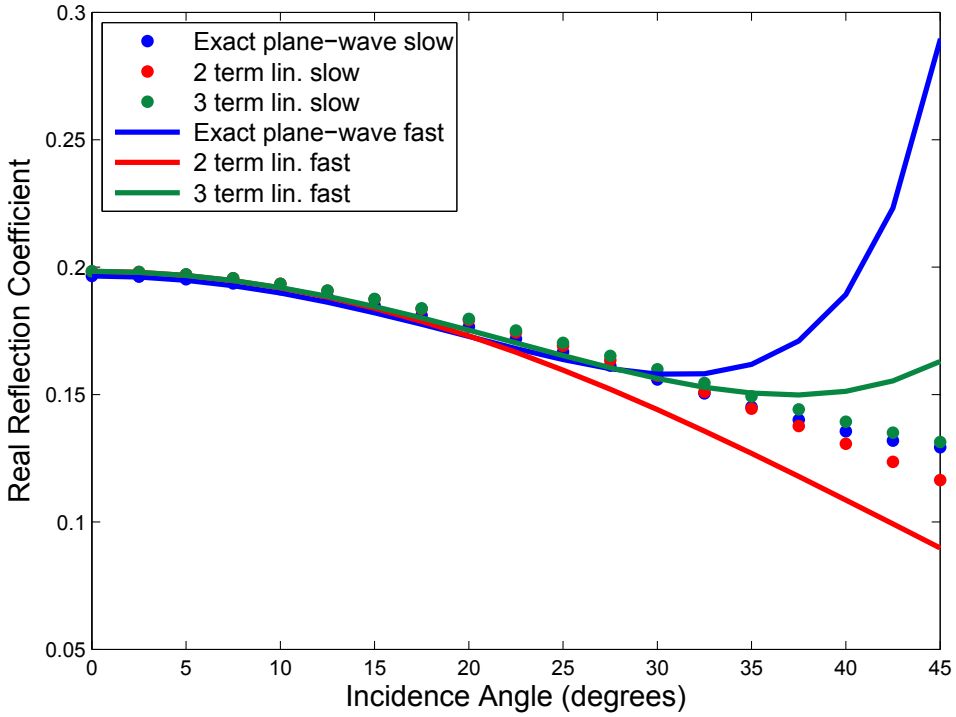

FIG. 6. Comparison of anisotropic reflection coefficient linearization to exact plane-wave coefficient. In blue are the exact plane-wave anisotropic reflection coefficients. In green are the linearizations from Vavryčuk and Pšenčík (1998) (eq. 4 in this paper), and in red are the linearizations using only the first two angle terms in eq. 4. The solid lines are for an azimuth of 90° which is the fast direction of the lower medium, representing the direction parallel to a fractured medium. The dotted lines are for an azimuth of 0° which is the slow direction of the lower medium, representing the direction perpendicular to a fractured medium. Using the all 3 terms, including the AVO curvature, more closely approximates the exact plane-wave reflection coefficient than just using 2 terms and in the fast direction in which there is a larger contrast in velocities, the 3 term linearization diverges around 30 degrees rather than at 20 degrees. For the fast direction, in which the contrast of elastic parameters across the layer is greater, the linearizations do not approximate the exact plane-wave equation well at large angles in the precritical region.

plane-wave equation well at large angles in the precritical region. We attribute this to the nonlinearity that occurs in the precritical region and the fact that increasingly higher order terms which can describe increasingly larger contrasts and angles are truncated in the linearization. In another CREWES report in this volume (Kolb et al., 2014) we create a series expansion of the exact plane-wave anisotropic reflection coefficient in order to analyze the nonlinearity present.

MARKOV CHAIN MONTE CARLO ANALYSIS

Because of the nonlinearity in the reflection coefficients and the inaccuracy it causes in the estimated stiffnesses, we decided to perform an inversion using exact reflection coefficients. We used a Markov chain Monte Carlo (MCMC) algorithm to analyze data from the slow and fast directions of the physical model. As input values to the algorithm we used the stiffnesses estimated from group velocities by Mahmoudian (2013) for the top layer (Table 2), and averaged the estimated stiffnesses for the lower layer (Table 1) to create an isotropic

starting model for the bottom layer as well. Priors were set as normally distributed with standard deviations of 10% of the stiffnesses for the top layer and standard deviations of 20% of the stiffnesses for the bottom layer. Densities were fixed to their known values for the tests in this report and we inverted for A'_{11}, A'_{13}, A'_{33}, and A'_{55} for each layer, resulting in 8 estimated parameters.

Figure 7 shows histograms of estimated horizontal P-wave velocities, V_{PH}, and S-wave velocities, V_S, for the slow and fast directions of the physical model, which are proportional to the posterior distributions (Metropolis et al., 1953). Using just the AVO gradient for anisotropy analysis results in a 90-degree ambiguity in the fracture direction, and using the AVO curvature gives a first order approximation to the velocities, but using the exact reflection coefficients for forward modeling, as done here, results in more accurate velocities, especially the horizontal P-velocity. Also, it can be seen that the S-velocity distribution is broader, meaning that there is more uncertainty on its estimate, likely due to the fact that it is coupled to a larger number of other elastic parameters in the AVO gradient.

Figure 8 shows histograms of the differences in vertical and horizontal P-velocities across the interface for the slow and fast directions. Since the P-impedance is well constrained and we fixed the density values, the difference in vertical P-velocity is also well constrained (see the x-axis). The reason there is error between the MCMC result and the group velocity estimate is likely because synthetics using the group velocity estimate don't fit the data due to: noise, an anomaly at small incidence angles, and possibly model error. Figure 9 shows the synthetic PP reflection coefficients using elastic parameters estimated from group velocities for the slow and fast directions of the physical model. Given that there is some misfit between the synthetics and the data, it makes sense that our estimated elastic parameters will have some misfit with the ones estimated from group velocities. Because at higher order there is nonlinear coupling between the horizontal velocity and other elastic parameters, the distribution for the change in horizontal P-velocity across the interface is broader than that for the change in vertical P-velocity; it cannot be completely constrained because other parameters can be varied along with it, resulting in similar reflection curves.

In Figures 10 & 11, we repeated our MCMC algorithm, but used equation 4, the linearization from Vavryčuk and Pšenčík (1998), as the forward model. The main difference in the results when using the linearized equation is that there is a larger error in both the horizontal P-velocity as well as the difference in horizontal P-velocities in the fast direction when compared to results using the exact reflection coefficient. This demonstrates once again the error in the estimation of the horizontal P-velocities when using a linearization of the PP reflection coefficient for a large contrast.

CONCLUSIONS

Formulating azimuthal AVO as a series of AVO inversions along different azimuths allows for an alternative representation of the theory. Typical inversion schemes assume symmetry of some sort and use it to provide a relation between the AVO gradient terms along different azimuths in order to simplify the problem. By allowing for arbitrary anisotropy, the media may be more realistic in some areas. Although it is not possible to invert for

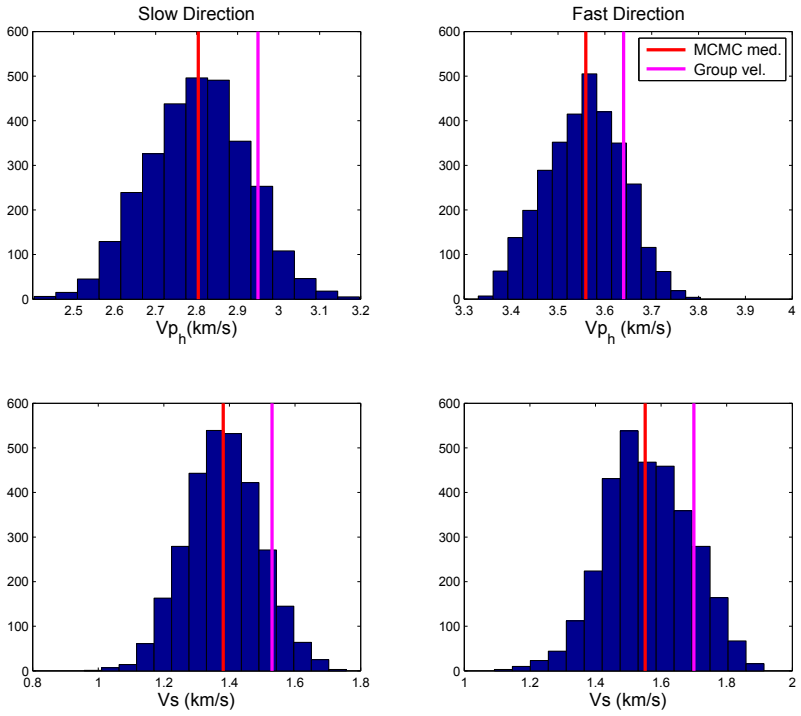

FIG. 7. Histograms showing posterior probability densities of velocities in the slow and fast directions of the physical model, using an exact forward model for the inversion. Red lines indicate the medians of the Markov chain values and magenta lines indicate the values estimated from group velocities by Mahmoudian (2013). (top) horizontal P-velocities. (bottom) S-velocities. (left) Slow direction. (right) Fast direction.

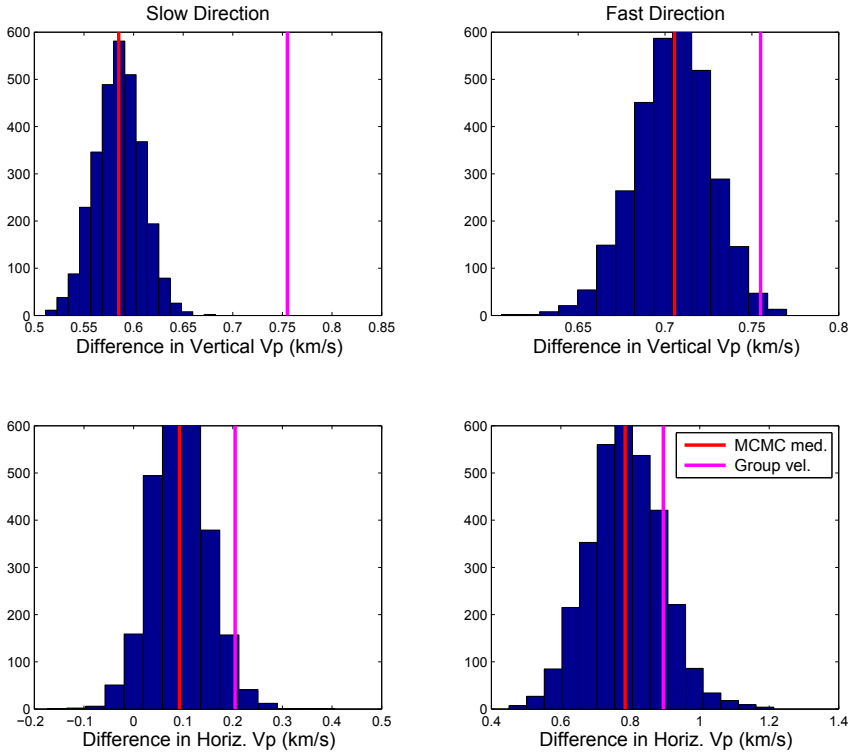

FIG. 8. Histograms showing posterior probability densities of the change in velocities across the interface in the slow and fast directions of the physical model, using an exact forward model for the inversion. Red lines indicate the medians of the Markov chain values and magenta lines indicate the values estimated from group velocities by Mahmoudian (2013). (top) Change in vertical P-velocities. (bottom) Change in horizontal P-velocities. (left) Slow direction. (right) Fast direction.

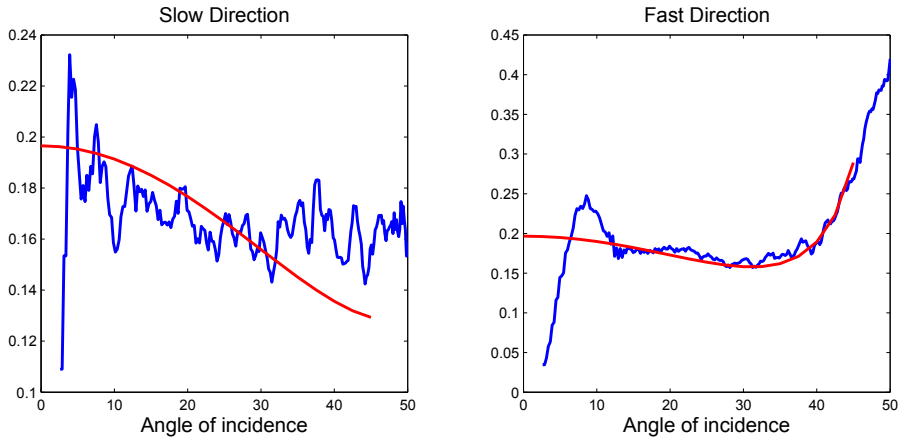

FIG. 9. PP reflection physical modeling data vs synthetics. (blue) PP reflection physical modeling data collected by Mahmoudian (2013). (red) Synthetic PP reflection curves using stiffnesses estimated from group velocities by Mahmoudian (2013). (left) Slow direction. (right) Fast direction.

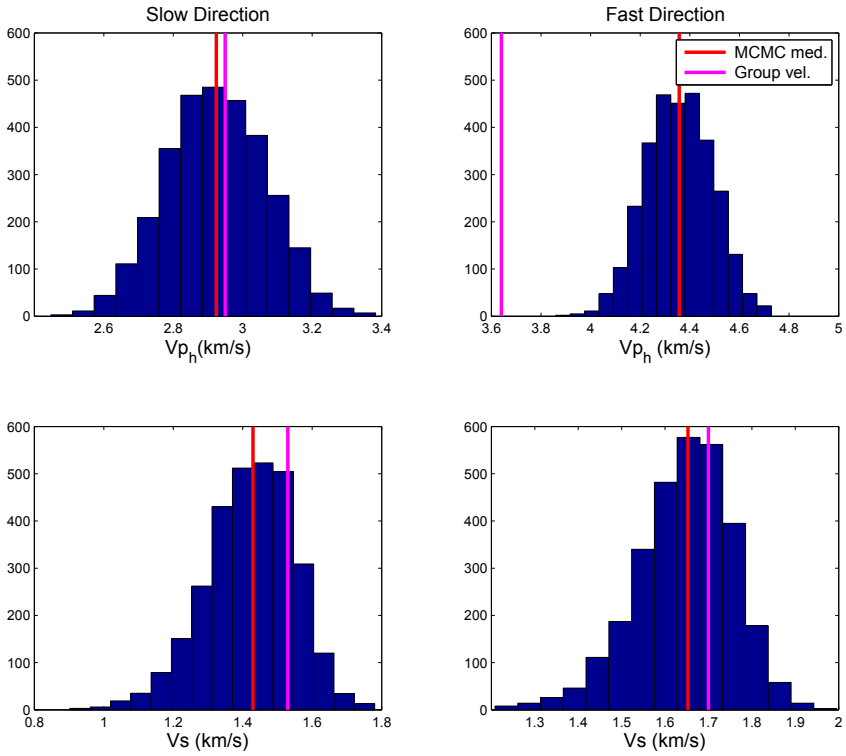

FIG. 10. Histograms showing posterior probability densities of velocities using the linearized forward model from Vavryčuk and Pšenčík (1998) (equation 4 in this paper). Red lines indicate the medians of the Markov chain values and magenta lines indicate the values estimated from group velocities by Mahmoudian (2013). (top) horizontal P-velocities. (bottom) S-velocities. (left) Slow direction. (right) Fast direction.

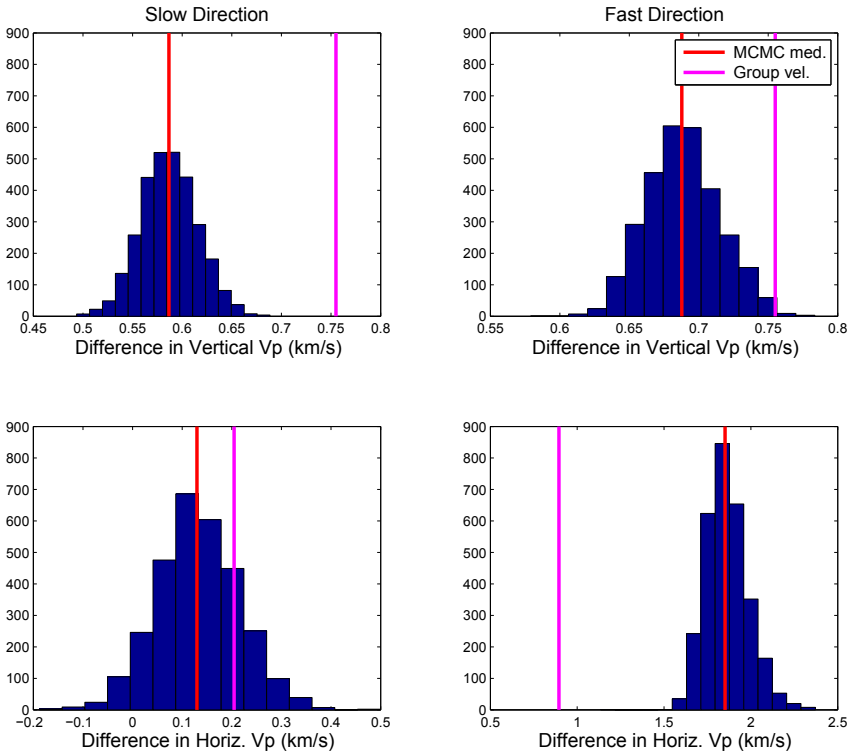

FIG. 11. Histograms showing posterior probability densities of the change in velocities across the interface using the linearized forward model from Vavryčuk and Pšenčík (1998) (equation 4 in this paper). Red lines indicate the medians of the Markov chain values and magenta lines indicate the values estimated from group velocities by Mahmoudian (2013). (top) Change in vertical P-velocities. (bottom) Change in horizontal P-velocities. (left) Slow direction. (right) Fast direction.

all the stiffness coefficients of a triclinic medium using PP reflection data, it is possible that allowing for arbitrary anisotropy and calculating stiffnesses along different azimuths may tell us which directions are more or less stiff, which could be useful information. Additionally, the AVO curvature is only dependent on one elastic stiffness, normalized by the background velocity, and this simplicity allows for it to estimate a change in stiffness uniquely, which could be useful on its own if the data quality is good, or as a constraint to alternative anisotropic methods such as using the AVO gradient. Furthermore, we showed that the curvature cannot accurately estimate horizontal P-velocities for a large contrast and is more useful as a constraint in these situations. Nonlinear inversion methods, such as the MCMC algorithm presented here, can be used if the horizontal P-velocities need to be estimated more accurately.

ACKNOWLEDGMENTS

We would like to thank Faranak Mahmoudian for allowing us to use physical modeling data from her thesis, which she both collected and processed. Also, the first author would like to thank Pat Daley and Khaled Al Dulaijan for discussions about this research. The work reported here was funded by CREWES and NSERC.

REFERENCES

Bakulin, A., Grechka, V., and Tsvankin, I., 2000, Estimation of fracture parameters from reflection seismic data-Part I: HTI model due to a single fracture set: Geophysics, **65**, No. 6, 1788–1802.

Bond, W. L., 1943, The mathematics of the physical properties of crystals: Bell system technical journal, **22**, No. 1, 1–72.

Castagna, J. P., and Backus, M., 1993, Offset-dependent refletivity-theory and practice of AVO analysis: Investigations in Geophysics series, **8**.

Gillespie, P., Howard, C., Walsh, J., and Watterson, J., 1993, Measurement and characterisation of spatial distributions of fractures: Tectonophysics, **226**, No. 1, 113–141.

Goodway, B., Perez, M., Varsek, J., and Abaco, C., 2010, Seismic petrophysics and isotropic-anisotropic AVO methods for unconventional gas exploration: The Leading Edge, **29**, No. 12, 1500–1508.

Hudson, J., 1981, Wave speeds and attenuation of elastic waves in material containing cracks: Geophysical Journal of the Royal Astronomical Society, **64**, No. 1, 133–150.

Jenner, E., 2002, Azimuthal AVO: Methodology and data examples: The Leading Edge, **21**, No. 8, 782–786.

Kolb, J., Innanen, K., and Cho, D., 2014, Series analysis of anisotropic reflection coefficients for inversion: CREWES Research Report, **26**.

Mahmoudian, F., 2013, Physical modeling and analysis of seismic data from a simulated fractured medium: Ph.D. thesis, University of Calgary.

Metropolis, N., Rosenbluth, A. W., Rosenbluth, M. N., Teller, A. H., and Teller, E., 1953, Equation of state calculations by fast computing machines: The journal of chemical physics, **21**, No. 6, 1087–1092.

Parney, R., Lange, N. et al., 2010, Comparison of seismic brittleness and anisotropy to micro-seismic in the waltman shale, *in* 2010 SEG Annual Meeting, Society of Exploration Geophysicists.

Prioul, R., Bakulin, A., and Bakulin, V., 2004, Nonlinear rock physics model for estimation of 3D subsurface stress in anisotropic formations: Theory and laboratory verification: Geophysics, **69**, No. 2, 415–425.

Rüger, A., 1995, P-wave reflections and azimuthal dependence of AVO in transversely isotropic media: Center for Wave Phenomena Res. Rep. CWP, **171**.

Rüger, A., 1998, Variation of P-wave reflectivity with offset and azimuth in anisotropic media: Geophysics, **63**, No. 3, 935–947.

Sayers, C. M., 2009, Seismic characterization of reservoirs containing multiple fracture sets: Geophysical Prospecting, **57**, No. 2, 187–192.

Schoenberg, M., and Sayers, C. M., 1995, Seismic anisotropy of fractured rock: Geophysics, **60**, No. 1, 204–211.

Shuey, R., 1985, A simplification of the Zoeppritz equations: Geophysics, **50**, No. 4, 609–614.

Thomsen, L., 1986, Weak elastic anisotropy: Geophysics, **51**, No. 10, 1954–1966.

Thomsen, L., 1990, Poisson was not a geophysicist!: The Leading Edge, **9**, No. 12, 27–29.

Thomsen, L., 1993, Weak anisotropic reflections: Offset-dependent reflectivity—Theory and practice of AVO analysis: Soc. Expl. Geophys, 103–111.

Tsvankin, I., Helbig, K., and Treitel, S., 2001, Seismic signatures and analysis of reflection data in anisotropic media.

Vavryčuk, V., and Pšenčík, I., 1998, PP-wave reflection coefficients in weakly anisotropic elastic media: Geophysics, **63**, No. 6, 2129–2141.

Zillmer, M., Gajewski, D., and Kashtan, B. M., 1998, Anisotropic reflection coefficients for a weak-contrast interface: Geophysical Journal International, **132**, 159–166.